# Vacuum-ultraviolet optical properties of single-crystal cadmium

C. G. Olson and D. W. Lynch

*Ames Laboratory, United States Atomic Energy Commission and Department of Physics, Iowa State University, Ames, Iowa 50010*

(Received 15 September 1972; revised manuscript received 11 July 1973)

The reflectivity of single-crystal Cd has been measured between 350 and 2500 Å using synchrotron radiation. The data have been Kramers-Kronig analyzed and corrections for an overlayer of CdO discussed. The imaginary part of the dielectric constant exhibits a sharp rise at about 9.35 eV due to the onset of transitions from the top of the 4*d* bands to the Fermi level. These transitions persist, with structure, to high energy, only about a third of their oscillator strength being used by 30 eV. The bulk and surface plasmon energies are found to be 8.80 and 7.30 eV.

## INTRODUCTION

This paper presents the results of measurements of the reflectivity of single crystals of cadmium in the vacuum ultraviolet. The use of the far-ultraviolet continuum provided by synchrotron radiation allowed the detection of structure in the reflectivity spectrum of Cd above 10 eV. The polarization of the radiation and the use of single crystals permitted a search for anisotropy in high-energy interband absorption and in the plasma frequency, but no anisotropy could be proven. A detailed description of the measurement system and data treatment is presented for its potential utility to other users of such radiation sources, and for reference in forthcoming presentations of data on other crystals.

Cd, a hexagonal metal, has a complex dielectric-constant tensor with two components, $\tilde{\epsilon}_{\parallel}$ and $\tilde{\epsilon}_{\perp}$, the $c$ axis being the reference. The spectra of these components have been measured in the infrared, visible, and near ultraviolet,[1,2] but not in the vacuum ultraviolet. In the latter region, phenomena related to plasmons and to the excitation of 4*d* "core" electrons to states above the Fermi level can be observed, and have been studied using thin films.[3-6] Some work has also been done on single crystals,[7] but less structure was observed than in our study.

In the following we report our reflectivity measurements on Cd, their subsequent Kramers-Kronig analysis, and the role a layer of CdO on the surface plays in the analysis. From the data we describe the bulk and surface plasmon in Cd, and show structure in the reflectivity and imaginary part of the dielectric constant that arises from the spin-orbit splitting of the 4*d* levels and from structure in the density of states above the Fermi level. The sum rule shows that by 30 eV, our high-energy limit, only about a third of the oscillator strength of the 4*d* electrons is exhausted.

## EXPERIMENTAL

Since many features of the apparatus are attempts to utilize unique features of synchrotron radiation from an electron storage ring,[8-10] a very brief review of its properties are in order. The light source was the 240-MeV electron storage ring at the Physical Sciences Laboratory of the University of Wisconsin. In contrast to that in a synchrotron, the electron beam in the storage ring is constant in energy and only slowly varying in magnitude, with a half-life of the order of 2 h. The radiation intensity is a maximum in the plane of the orbit, with a vertical divergence that decreases at shorter wavelengths. In the orbital plane the radiation is completely polarized. Above and below this plane, the degree of polarization decreases and is wavelength dependent.

The beam from the storage ring is focused on the entrance slit of the monochromator using a 3.5° grazing-incidence elliptical mirror[11] which provides a 2:1 reduction. This design permits the use of a narrow entrance slit and increases the divergence of the beam to fill the grating. A plane mirror after the elliptical mirror restores the beam to horizontal. The chamber housing the mirrors also acts as a vacuum separation chamber between the $10^{-10}$ Torr in the ring and the $10^{-7}$–$10^{-8}$ Torr in the monochromator.

The monochromator is an ion-pumped McPherson 225 (1-m, normal incidence) used primarily with a 1200-line/mm ($Al+MgF_2$)-coated grating. Even though the reflectivity of the grating drops at high energy, the intensity of the synchrotron radiation is increasing and the combination is useful to 350 Å. Two minor modifications have been made. A gearbox was added to allow the monochromator to be driven either by the synchronous motor or by a stepping motor. A 40-turn potentiometer was added to give an analog readout of the wavelength.

Now refer to Fig. 1. In the monochromatic beam, the beam splitter serves several purposes. It is an inclined plate with a 1-mm hole. The area surrounding the hole is coated with a phosphor (sodium salicylate) and radiation striking this provides a monitor signal. The hole is also the limiting aperture in the beam, passing about 8 mrad of

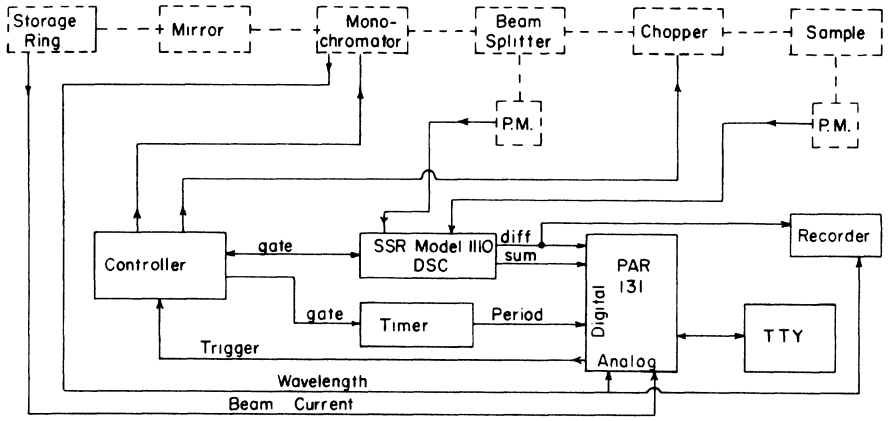


FIG. 1. Block diagram of the measurement system. See text for description.

beam. (Because of the focusing mirror, this is 4 mrad as emitted by the storage ring.) Since the vertical spread of low-energy radiation is greater than that of the high, this aperture if accurately aligned, discriminates against low-energy radiation. The plate also blocks a great deal of the scattered radiation. In addition, by limiting the vertical acceptance, the polarization is kept high. This aperture is sufficiently small that at 760 Å the scattered (including zero-order) radiation is reduced from several percent to well under $\frac{1}{4}\%$. Generally no correction for scattered light need be made.

Following the beam splitter is a stepping-motor-driven chopping wheel containing both opaque and alkali-halide choppers. At short wavelengths, the reflectivities of the grating and sample favor the long-wavelength stray light. Use of a LiF chopper allows us to reject dark counts and long-wavelength stray light. A linear-motion feedthrough allows thin-film filters to be positioned in the beam.

The remainder of the sample chamber is shown diagrammatically in Fig. 2. The sample holder assembly rests on a ring (*A*) which is fixed to the chamber wall. The adjustment of the ring with respect to the wall and the plate (*B*) with respect to the ring allows the axis of the shaft (*D*) to be positioned normal to and intersecting the beam. The sample mount (*E*) is adjusted to put the axis of rotation in the face of the sample. The position of plate (*B*) with respect to the ring is determined by the alignment screws, so that the sample may be aligned and then removed from the chamber for etching just prior to pump down.

For alignment the chamber is removed from the monochromator and a laser positioned normal to, and centered on, the front flange of the chamber. The beam splitter, chopper, and baffles are positioned and the sample adjusted. Later, when the sample chamber is coupled to the exit slit and evacuated, the chamber can be aligned as a unit with respect to the beam.

The detector is either a Bendix channeltron or, as shown, a 1P21 photomultiplier with phosphor. The 1P21 is mounted horizontally and a rectangular hood placed above it with the phosphor on the back, inclined, surface. The interior of the hood acts as an integrating chamber for the visible light and makes the detector less position sensitive. The acceptance angle is only slightly larger than the beam so that the detector is not sensitive to

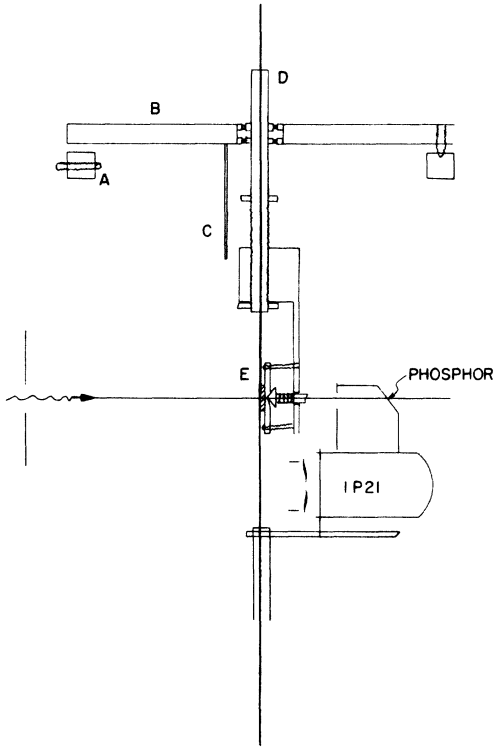


FIG. 2. Reflectometer. *A*: mounting ring; *B*: plate; *C*: stop for raising sample; *D*: rotatable shaft; *E*: sample mount.

light scattered off the walls of the sample chamber. The narrow hood allows the detector to be close to the incident beam and angles of incidence between 7° and 80° on either side of normal incidence may be used. Continued rotation of the shaft ($D$) with the sample holder against the stop ($C$) moves the sample vertically in and out of the beam, allowing the incident beam to be measured.

The portion of the sample chamber containing the sample and detector can be rotated, under vacuum, about a horizontal axis to change the polarization with respect to the sample. This allows anisotropic crystals to be studied.

The reflectivity of a bicrystal of indium was measured, using the photomultiplier and phosphor as detector. This combination is more sensitive to stray light than is the channeltron. Indium has a reflectivity minimum at 740 Å. The value of the reflectivity at this minimum depends on the amount of oxide on the surface, and our sample had some oxide. The important feature is that the minimum reflectivity of our sample had the remarkably low value of 0.0003. If there were much long-wavelength scattered light present, this value would have been erroneously measured as much higher. At higher photon energies, reflectivity measurements were made both with and without an Al thin-film transmission filter, with identical results. Even at 30 eV, scattered light with energies below about 15 eV is negligible. Second-order light was also not a problem in the work on Cd.

Data acquisition is based on a SSR model 1110 Digital Synchronous Computer.[12] It is most commonly used in the chopper mode with the monitor signal as an external clock. A data sequence would be:

(1) Position the chopper—LiF or stainless steel depending on the wavelength.

(2) Count dark and stray light pulses until a preset number of counts had been accumulated from the monitor. This means that the cycle time is a function of beam current and wavelength. A second counter timer measures the duration of the count cycle. This allows one to determine the monitor count rate and is valuable for error analysis, diagnostics, and to correct for monitor dark count if necessary.

(3) A gate-closing signal from the 1110 triggers the stepping motor which moves the chopper to the open position.

(4) Count into a second channel the true, dark, and stray light pulses, again until a preset number of counts have been received from the monitor.

(5) The 1110 computes the sum and difference of the channels, the difference being the number of true counts, and triggers the readout cycle of the PAR 131 data handling system.[13]

(6) At each point a teletypewriter records the wavelength, the electron current in the storage ring, the sum and difference count, and the cycle time. The difference count is also fed to a $D/A$ converter in the 1110 and displayed on a strip chart.

(7) A signal from the PAR 131 during the print cycle triggers an advance of the wavelength and restarts the measurement cycle. Hence data may be accumulated while the previous point is being read out.

Separate wavelength scans are made of the incident beam ($I_0$) and reflected beam. Because of the stability of the source and the use of the beam splitter, several different reflectivity runs may be made for each $I_0$, resulting in a great improvement in efficiency. Also, using the monitor as the time base normalizes the runs for beam decay as well as reduces the effect of change in intensity as a function of wavelength. The normalization for the wavelength dependence of the $I_0$ is not perfect because the portion of the beam that is transmitted by the beam splitter is weighted to short wavelengths. Nevertheless, the $I_0$ spectrum is flat enough so that the approximate reflectivity can be determined from the strip chart. Accurate determination of $R$ requires a division by $I_0$. For a few runs this can be done from the printed teletype output. The major data reduction is done off-line using the paper tape from the teletype and an IBM 360/75.

The method described is the most commonly used, but by no means the only one. The sample holder can be replaced by a cryostat holding liquid nitrogen or helium. This limits the reflectivity to a single angle and $p$ polarization, but several samples can be loaded at one time. Electronically, the chopping mode is not always used. If dark counts and long-wavelength stray light are not a problem (as with a channeltron), pulses from the two detectors may be counted simultaneously in the two channels of the 1110, and the analog measure of the beam current used for later normalization.

## CRYSTALS

Single crystals of Cd were either spark cut or acid cut. Most were spark cut, mechanically polished, etched (66.7 g $CrO_3$ and 5 g $Na_2SO_4$ in 333 ml $H_2O$), then lightly repolished and etched just before placing in the vacuum of the sample chamber ($10^{-7}$ Torr). The best sample, whose surface was a basal plane, was acid cut and acid polished ($HNO_3$). The principal concern was to minimize strain in the surface region. The price paid for this was some oxide on the surface and a somewhat wavy surface, since the acid etch or polish on Cd leaves a less flat surface than do

electropolishes on many other metals. We do not know of a general way that one can obtain a single-crystal surface in a good vacuum that is oxide free and unstrained, especially one that is not a close-packed plane. Thermal etching and argon bombardment leave pits in the surface, and the latter also leaves a strained surface. Cleaving is occasionally a possibility, but usually only close-packed faces of noncubic crystals can be obtained.

## RESULTS

Figure 3 shows the reflectivity from the two best runs on Cd crystals. Other runs have the same structure beyond 10 eV, but with a generally reduced reflectivity magnitude. These were judged to have more deformed and/or oxidized surfaces (see below). Mechanically polished unetched surfaces also showed a rise in reflectivity at 10 eV, but the plasma edge below 10 eV had a less precipitous slope, and the minimum reflectivity was higher and located at higher energy. The structure above 10 eV shown in Fig. 3 is reproducible and believed to be real, but the magnitude of the reflectivity of the basal-plane sample probably is still below the true value for an ideal clean surface. Data taken with an Al transmission filter show that the rise in reflectivity at 28 eV is genuine, not produced by scattered light.

The three spectra in Fig. 3 have similar shapes but different magnitudes. We believe this is due to the rougher surface produced by the etch on the sample with the $c$ axis in the face. Some of the reflected light for this sample probably misses the detector and the fraction that misses changes when the sample is rotated to change the relative polarization. We have found no structure in the reflectivity that is anisotropic. Subsequent Kramers-Kronig analysis of the data in Fig. 3 will show that above 10 eV the real part of the refractive index $n - ik$, exceeds unity by less than 15% and the imaginary part is less than 0.4. Then, approximately, $\epsilon_1 \approx 1 - k^2$, $\epsilon_2 \approx 2k$, $R \approx \frac{1}{4} k^2$. This leads to $\epsilon_2 = 4\sqrt{R}$ to within 25%. The square root shows why the structure is more prominent in $R$ than in $\epsilon_2$.

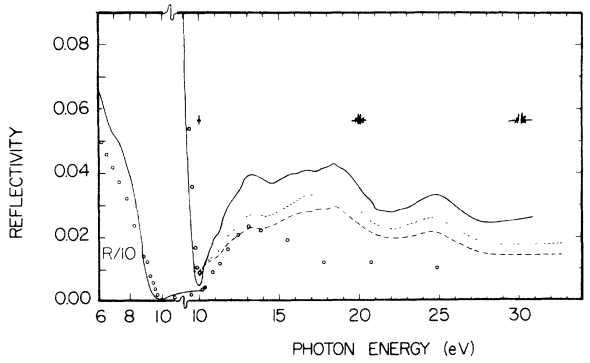


FIG. 3. Reflectivity of single-crystal Cd at 10° angle of incidence. Solid: basal plane, acid-cut, acid-polished sample, $p$ polarization. (At low energy $R/10$ is plotted. Note break in energy scale.) Dashed: spark-cut, acid-polished, etched sample $\vec{E} \perp \hat{c}$, $p$ polarization. Dotted: same sample but $\vec{E} \parallel \hat{c}$, $s$ polarization. The spectral bandpass is indicated with arrows. The circles are the reflectivity calculated from $n$ and $k$ values in Ref. 6.

## DATA TREATMENT

The reflectivity spectrum of the best Cd sample was Kramers-Kronig (KK) analyzed, taking into account the actual angle of incidence, but assuming perfect polarization of the radiation. (The actual measured degree of polarization at the sample was 88%.) In order to do so, available infrared and visible data[1] were used, with a Drude-like extrapolation to zero energy. The requisite extrapolation for energies higher than $E_0$, the highest for which data exist, cannot be made with confidence. Neither the commonly used power law, $R = R_0(E_0/E)^\alpha$, with $\alpha$ chosen by some criterion, nor the reflectivity of a free-electron gas in the high-energy limit, $R = R_0(E_0/E)^4$, can be used here because the reflectivity is rising, not falling, at our highest energy. Moreover, the sum rule will show that only about a third of the oscillator strength of the $4d$ electrons has been used below our high-energy limit. Of necessity, several high-energy extrapolations were used. These extrapolations are shown in Fig. 4 and their effects on the resultant real and imaginary parts of the dielectric constant are shown in Figs. 5 and 6. These extrapolations are discussed further in Appendix A.

The different extrapolations also affect the electron energy-loss function, $\mathrm{Im}(-1/\tilde{\epsilon})$. For extrapolations 1, 3, and 4 the position of the peak due to the excitation of volume plasmons is 8.76, 8.76, and 8.80 eV, respectively, while the peak height of the loss function is 3.87, 4.18, and 3.34, respectively. It is clear that the structures in $\epsilon_2$ are not affected greatly by the extrapolation uncertainty, but the magnitudes are strongly dependent on the form of extrapolation used. The position of the edge in $\epsilon_2$ depends slightly on the extrapolation. In the following analysis and in the discussion we arbitrarily have chosen to use the results of the KK analysis using the extrapolation labeled 4 in Fig. 4. (Extrapolation No. 3 is the least reasonable in our view.)

The KK analysis just described gives the phase of the amplitude reflectivity from the spectrum of its absolute value. The complex amplitude reflectivity $\tilde{r}$ could then be found. If there were no oxide layer, then the complex refractive index $\tilde{N}$ and the complex dielectric constant $\tilde{\epsilon}(\tilde{\epsilon} = \tilde{N}^2)$ of the

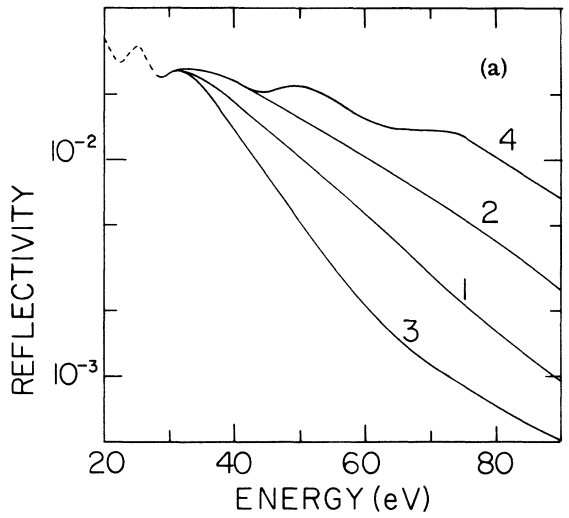


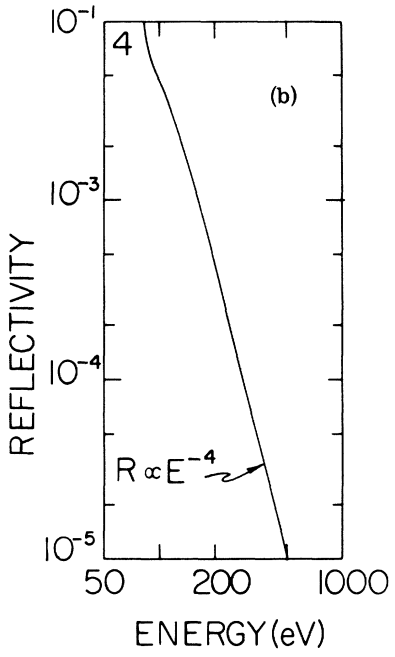


FIG. 4(a). High-energy extrapolations used in Kramers-Kronig analysis. The dashed line is actual data. (b) Continuation of (a).

metal can be found from $\tilde{r}$ by solving Eq. (1) for $\tilde{N}$:

$$\tilde{r} = (\tilde{g} - g_0)/(\tilde{g} + g_0), \tag{1}$$

in which $g_0 = \cos\phi_0$ and $\phi_0$ is the angle of incidence. $\tilde{g} = \tilde{N}\cos\tilde{\phi}$ for $s$ polarization and $\tilde{g} = \cos\tilde{\phi}/\tilde{N}$ for $p$ polarization. The complex angle $\tilde{\phi}$ is obtained from

$$\tilde{N}\sin\tilde{\phi} = \sin\tilde{\phi}_0 .$$

These relationships were used to obtain the spectra displayed in Figs. 5 and 6. They are valid at any angle of incidence, but assume complete polarization. If they were to be used on data taken with imperfect polarization. the degree of polarization would have to be known. For near-normal incidence the correction for our 88% polarization is negligible.

If there is an oxide layer of thickness $d$ and complex refractive index $\tilde{N}_1$, the foregoing is incorrect. If $d$ and $\tilde{N}_1$ are known, the unknown complex refractive index of the metal, now designated by $\tilde{N}_2$, can be found from $\tilde{r}$ by a more complicated expression[14] for $\tilde{r}$:

$$\tilde{r} = \frac{(\tilde{g}_2 - \tilde{g}_1)(\tilde{g}_1 + g_0)e^{\tilde{X}} + (\tilde{g}_2 + \tilde{g}_1)(\tilde{g}_1 - g_0)e^{-\tilde{X}}}{(\tilde{g}_2 + \tilde{g}_1)(\tilde{g}_1 + g_0)e^{\tilde{X}} + (\tilde{g}_2 - \tilde{g}_1)(\tilde{g}_1 - g_0)e^{-\tilde{X}}} . \tag{2}$$

Here

$$\tilde{X} = \frac{i\omega d}{c}\tilde{N}_1\cos\tilde{\phi}_1 ,$$

$$\tilde{N}_i\sin\tilde{\phi}_i = \sin\tilde{\phi}_0 \quad (i = 1, 2),$$

$$\tilde{g}_i = \tilde{N}_i\cos\tilde{\phi}_i \text{ for } s \text{ polarization},$$

$$\tilde{g}_i = (\cos\tilde{\phi}_i)/\tilde{N}_i \text{ for } p \text{ polarization},$$

and $\omega$ is the angular frequency. Equation (2) can be solved for $\tilde{N}_2$, but since we had values of $\tilde{N}^2$ from Eq. (1) already on punched cards, we equated (1) and (2), and solved for $\tilde{N}_2$ in terms of $\tilde{N}$ (which is no longer the complex refractive index of the metal), $\tilde{N}_1$, and $d$, getting

$$\tilde{g}_2 = \frac{\tilde{g}\tilde{g}_1}{g_0}\frac{(\tilde{g}_1 + g_0)e^{\tilde{X}} - (\tilde{g}_1 - g_0)e^{-\tilde{X}}}{(\tilde{g}_1 + g_0)e^{\tilde{X}} + (\tilde{g}_1 - g_0)e^{-\tilde{X}}} , \tag{3}$$

$$\tilde{N}_2^2 = \tilde{g}_2^2 + \sin^2\phi_0 \text{ for } s \text{ polarization}, \tag{4}$$

$$\tilde{N}_2^2 = [1 + (1 - 4\tilde{g}_2^2\sin^2\phi_0)^{1/2}]/2\tilde{g}_2^2 \tag{4'}$$

for $p$ polarization.

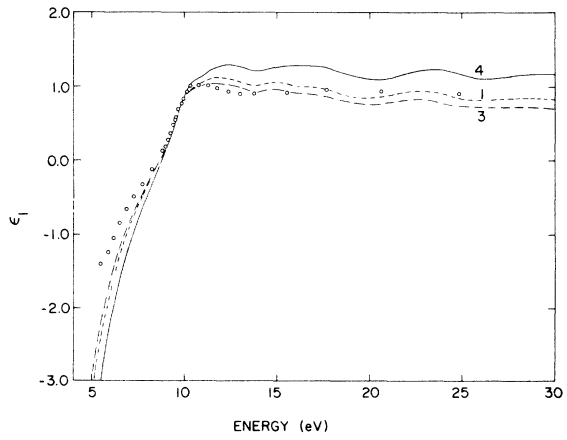


FIG. 5. Real part of the dielectric constant of Cd for $\vec{E}$ in the basal plane. Curves obtained by Kramers-Kronig analysis of the solid curve in Fig. 3 using extrapolations of Fig. 4. The circles are calculated from $n$ and $k$ values given in Ref. 6.

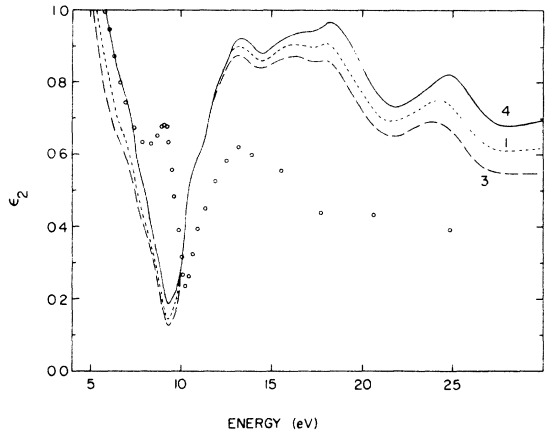


FIG. 6. Imaginary part of the dielectric constant of Cd for $\vec{E}$ in the basal plane. Curves obtained by Kramers-Kronig analysis of the solid curve in Fig. 3 using extrapolations of Fig. 4. Circles are calculated from $n$ and $k$ values given in Ref. 6.

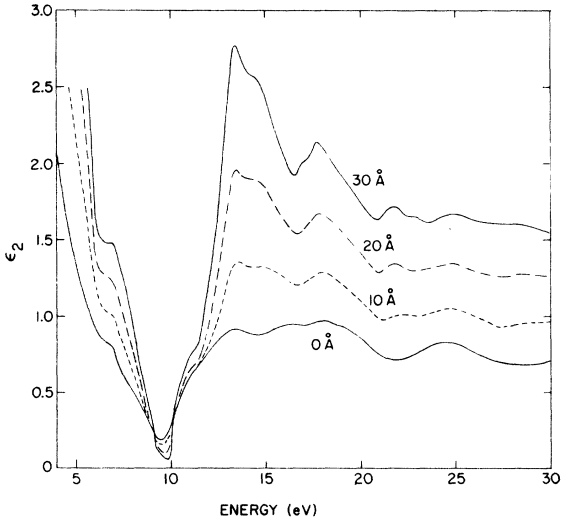


FIG. 8. Imaginary part of the dielectric constant of Cd for $\vec{E}$ in the basal plane corrected for 0, 10, 20, and 30 Å of overlying CdO.

$\tilde{N}_1$, the complex refractive index of CdO in our case, was obtained from a KK analysis of the reflectivity of single-crystal CdO. The data were those of Altwein *et al.*[15] in the visible and near infrared, Osmun[16] in the vacuum uv to about 20 eV, and our own reflectivity data on Osmun's crystal from 20 to 30 eV (Fig. 7). The thickness $d$ is unknown, so several values were assumed: 10, 20, and 30 Å. Figures 8 and 9 show the spectra of $\epsilon_2$ (now the imaginary part of $N_2^2$) and the electron energy-loss function, $\mathrm{Im}(-1/\tilde{\epsilon})$, obtained from Eqs. (1), (3), and (4′) for these three thicknesses. One of these curves represents the correct values for oxide-free Cd *if* the thickness of oxide actually were 0, 10, 20, or 30 Å. The obvious way to determine the thickness is to repeat this analysis with data taken at another angle of incidence and find the value of $d$ for which the spectra are identical, but because of the wavy nature of the heavily etched surface, we believe there are geometrical errors that make the magnitude of the reflectivity at larger angles less reliable than that for 10°. Further discussion of Fig. 8 is given in Appendix B.

One needs a criterion for setting an upper bound on $d$. There is a peak in $\epsilon_2$ of CdO at 8.0 eV. This peak and the associated structure in $\epsilon_1$ of CdO give rise to a peak at 7 eV on the plasma edge of $\epsilon_2$ for corrected Cd (Fig. 8), a peak which increases as $d$ increases. When $d = 50$ Å, this peak is well resolved from the edge. We assume that metallic Cd has no such *sharp* (FWHM $\lesssim 1.0$ eV) peak, and

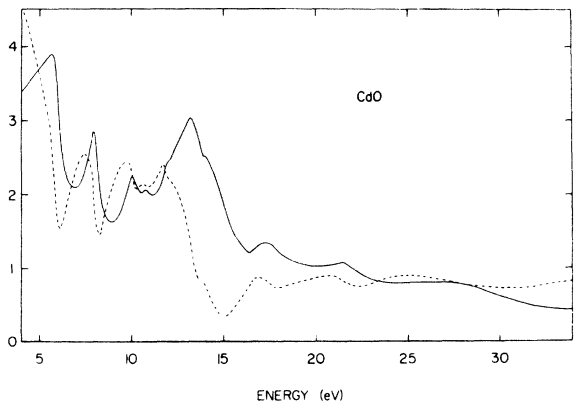


FIG. 7. Real and imaginary parts of the dielectric constant of CdO used to calculate the effect of CdO overlayers on the dielectric constant of Cd. Solid: $\epsilon_2$; dashed: $\epsilon_1$.

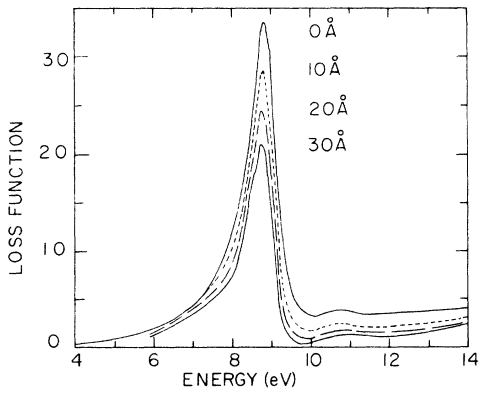


FIG. 9. Electron energy-loss function $\mathrm{Im}(-1/\tilde{\epsilon})$ of Cd for $\vec{E}$ in the basal plane corrected for 0, 10, 20, and 30 Å of overlying CdO.

that its occurrence at 7 eV is the result of correcting for a larger thickness of oxide than actually was present. To determine a criterion for limiting $d$, we show in Fig. 10 the reflectivity of hypothetical oxide-free Cd as calculated from the spectrum of $\tilde{N}_2$ for various values of $d$. One of these curves would be the correct reflectivity of an oxide-free crystal if our data in Fig. 3 were taken with 0, 10, 20, or 30 Å of CdO present. The previously mentioned peak in $\epsilon_2$ appears as a dip in the reflectivity between 6.5 and 8 eV. How large a dip is consistent with our estimated errors? The curve for 10 Å of CdO is nearly indistinguishable from the original curve—both depart from the average of the two by only 0.01 reflectivity unit. The curves for 20 and 30 Å have more noticeable dips and probably represent "overcorrected" curves. The same can be said about the peaks at 6.0 eV. On the premise that these structures are caused by CdO, we believe that our best sample had less than 20 Å of oxide present during the measurements. The dip in the reflectivity of "oxide-free" Cd between 6.5 and 8 eV (Fig. 10) is the result of the correction. If we reverse the order of calculation and ask for the role of an increasing thickness of oxide layer on the measured reflectivity, we find it is the opposite of the effects portrayed in Figs. 8–10. It is an increase in the reflectivity near 7 eV, turning into a peak for large values of $d$, a filling in of the minimum near 9.5 eV, and a decrease in the magnitude of the reflectivity above 10 eV. All of these effects were observed on the other samples, to different extents, depending on the amount of oxide present. Thus we believe that our best sample had the least oxide, a layer estimated not to exceed 20 Å.

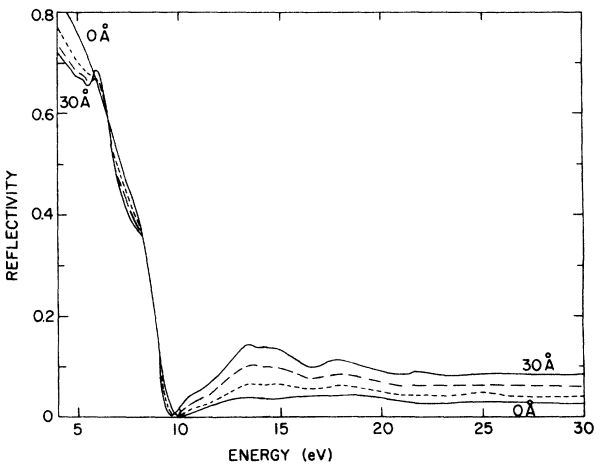


FIG. 10. Reflectivity of Cd for $\vec{E}$ in the basal plane corrected for 0, 10, 20, and 30 Å of overlying CdO. One of these curves would represent the reflectivity of oxide-free Cd if the actual oxide thickness present in the sample in Fig. 3 were 0, 10, 20, or 30 Å.

Still, a layer as thin as 10 Å has a dramatic effect on the magnitudes of the complex dielectric constant. Moreover, the peaks in $\epsilon_2$ at 7.0, 13.5–15.0, 17.8, and 21.8 eV (Fig. 8) all grow with correction for increasing oxide thickness. Their great sharpness in the curve corrected for 30 Å of CdO makes this seem like an overcorrection for the actual oxide. Application of the sum rule to Fig. 8 yields 3.2 electrons/atom contributing to the absorption between 9.5 and 30 eV when no oxide correction is applied, while the correction for 10 and 20 Å of CdO yields 4.4 and 5.7, respectively, for this quantity. In all cases the oscillator strength of the ten $4d$ electrons is not exhausted by 30 eV.

## RESULTS AND DISCUSSION

It is difficult to assess errors in vacuum-ultraviolet measurements of the reflectivity. The reflectivity can be measured to within a few percent, but the problem is how closely do the measured values represent the reflectivity of an ideal flat strain-free surface. The effects of an oxide are a general decrease in the reflectivity at high energy and a shallower minimum in the reflectivity for Cd. The effect of strain should be a broadening of structure, usually reducing peak heights. Thus, in comparing our results with those of others, we can say that since our high-energy reflectivity values are higher, they are closer to those of an ideal surface, but how close we cannot say. Additional errors introduced by the KK analysis were estimated in connection with Figs. 5 and 6. It is interesting to note that most of the preceding papers on the vacuum ultraviolet properties of Cd contain no discussion of errors, other than those in the original measurement.

Probably the best previous data on Cd is by Jelinek *et al.*[6] using the multiple-angle reflectivity method on films, some of which were transferred between vacuum chambers and some of which were evaporated *in situ* at about $10^{-6}$ Torr. Their data are shown in our Figs. 3, 5, and 6 as circles. There is no way that the effect of an oxide film on our samples can account for the discrepancies, but we have not analyzed their method for the role of an oxide film. Thus it is still possible that oxide layers on both samples could reconcile the differences. However the peak in $\epsilon_2$ and the structure in the reflectivity near 9.0 eV in their data probably will not be explained by such an analysis, so this discrepancy probably will remain. Except for the 9.0-eV structure, the shapes of both sets of spectra are in general agreement. The errors in the magnitudes of $n$ and $k$ and $\epsilon_1$ and $\epsilon_2$ resulting from KK analysis tend to be much larger than the

errors in the reflectivity measurements and may easily reach 50%. Errors in $\epsilon_2$ due to the oxide can also reach 50% (Fig. 8). The shapes of the spectra of $\epsilon_1$ and $\epsilon_2$ are less affected by such errors, and we proceed to discuss these.

The sharp rise in $\epsilon_2$ at 9.35 eV is due to the onset of interband transitions from the upper-spin-orbit-split $4d$ level to the Fermi level. The position of the onset varies between 9.30 and 9.40 eV for various high-energy reflectivity extrapolations (no oxide corrections), and between 9.35 and 9.80 eV for corrections for from 0 to 30 Å of CdO with the fourth reflectivity extrapolation. The value of 9.35 eV is in near-perfect agreement with the results of x-ray photoelectron spectroscopy.[17] Structure in the reflectivity above the onset of $4d$ transitions is complicated by the onset of transitions from the lower spin-orbit-split $4d$ level. Pollack *et al.*[17] have studied the $4d$ levels in Cd and have found them to be somewhat broadened by the lattice potential, and to have a spin-orbit splitting of 1.0 eV, compared with values calculated for free atoms[18,19] of 0.90 and 0.79 eV. Moreover, the ratio of the degeneracies was closer to 1.3:1 instead of the 1.5:1 expected. High-resolution ultraviolet-photoemission results have recently been reported.[20-22] They place the $4d$ levels of Cd at 10.20 and 11.15 eV below the Fermi level, and the full width at half-maximum for the broadened "total" $4d$ band is given as 1.69 eV. The spin-orbit splitting of 0.95 eV is in good agreement with the data obtained by x-ray photoelectron spectroscopy, both of which indicate the splitting is larger in the metal than that calculated and measured (0.7 eV)[23] in the free atom. The weights of the two components is approximately 1.5:1.[21]

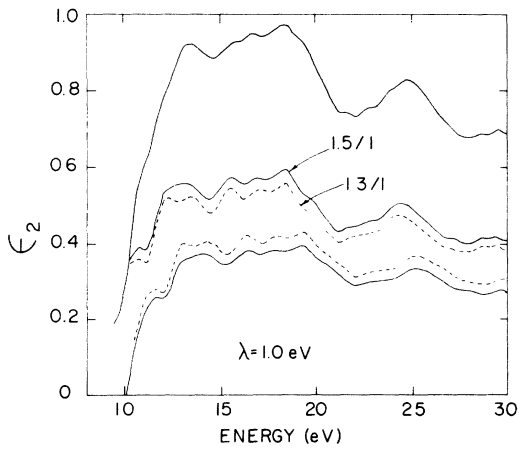


FIG. 11. Decomposition of $\epsilon_2$ (from reflectivity extrapolation 4 with no oxide correction) into two spin-orbit components with splitting 1.0 eV and relative weights of 1.5:1 (solid) and 1.3:1 (dashed). The uppermost curve is the total $\epsilon_2$.

In Fig. 11 we have decomposed our $\epsilon_2$ spectrum into two components. The splitting assumed was 1.0 eV and two relative weights, 1.5:1 and 1.3:1, were used. No broadening of the $4d$ levels was used. Considerable structure is revealed. This structure would be enhanced by any correction for CdO. It is known[24,25] that the electric dipole matrix element should not give rise to much structure in $\epsilon_2$, but only to features varying slowly with energy. Insofar as a $4d$ sublevel is not broadened by solid-state effects, the $\epsilon_2$ component arising from one of the two sublevels is proportional to the product of a squared matrix element and the density of final states, the latter being approximately the density of $p$-like states just above the Fermi level. (Correction for the finite width of the two $4d$ levels would further enhance the structure we report in the density of final states.) The most reliable band structure[26] for Cd stops at 3 eV above $E_F$, so identification of the peaks in Fig. 11 is difficult. The structures in Fig. 11 do not have the canonical shapes associated with critical points, but because there are apparently no low-lying flat bands in Cd and the initial states are in a fairly narrow band, critical points, possibly in groups, should be involved. There are a number of $M_0$-type critical points at $H$ that lie between 0.7 and 1.5 eV above $E_F$,[26] which could contribute to the first peak that lies 1.5 eV above the onset of the edge in Fig. 11. The second peak is 3 eV above the onset, and that is the limit of the band calculations.

The density of empty states just above the Fermi level has also been studied by x-ray isochromat spectroscopy.[27,28] In that work the resolution was of the order of 0.5 eV. There are some differences between the two studies of Cd by this method. The second[28] shows peaks in the density of states at approximately 2.0, 7.7, and 12 eV above $E_F$. These do not resemble the structure in our Fig. 11. Our structures become weaker above a few eV beyond threshold, probably due to lifetime broadening. Definitive analysis of the structure in Fig. 11 awaits calculations similar to those done on Al to very high energies.[29,30] The $4d$ levels give rise to transitions to $p$-like and $f$-like final states. The former transitions tend to be concentrated near threshold, while the latter persist to very high energy,[31] leading in this case, to only about a third to one-half of the $4d$ electrons producing absorption below 30 eV.

Our loss function peaks at 8.80 eV, independent of the oxide correction. The peak height of 3.36 (extrapolation 4 and no oxide correction) is altered by the extrapolation used and by the oxide. In all cases, however, it is higher than that reported by Huebner *et al.*,[6] but it displays the asymmetry that their peak shows. See Fig. 12. Feuerbacher and

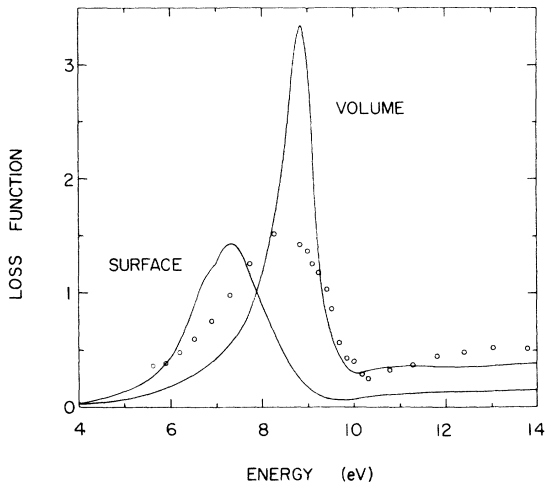


FIG. 12. Electron energy-loss function $\mathrm{Im}(-1/\tilde{\epsilon})$ and surface loss function, $\mathrm{Im}[-1/(\tilde{\epsilon}+1)]$ for Cd calculated from the $\tilde{\epsilon}$ obtained with reflectivity extrapolation 4 and no oxide correction. The circles are values of $\mathrm{Im}(-1/\tilde{\epsilon})$ calculated from the $n$ and $k$ of Ref. 6.

Fitton[32] have presented a table of all the measurements of the peak position and width of the plasmon in Cd. Our value for the peak position, 8.80 eV, is in best agreement with their own measurement of 8.68 eV, using photoemission. (The spread of reported values is very large.) The ratio of the half-wdith to the peak position that we obtain using no oxide correction is 0.091, in excellent agreement with the 0.092 obtained by Feuerbacher and Fitton, but considerably smaller than that obtained earlier by others.

The function $\mathrm{Im}[-1/(\tilde{\epsilon}+1)]$, called the surface loss function, is proportional to the probability that a fast electron will excite a surface plasmon, peaks in it occurring at surface-plasmon energies. For Cd we find a peak of height 1.44 at 7.30 eV (Fig. 12). Characteristic energy-loss measurements[33,34] show a single peak at 7.8 or 7.5 eV, possibly the result of both surface and bulk plasmons. The second peak observed in such measurements, a broad one at 15.1 eV, corresponds to no structure at all in the loss function and probably is the result of creation of two plasmons.

## ACKNOWLEDGMENTS

We wish to thank M. J. Murtha for acid cutting and acid polishing our crystal and the staff of the storage ring for their cooperation, especially E. M. Rowe, C. H. Pruett, and R. Otte. The storage ring is supported by the U. S. Air Force Office of Scientific Research.

## APPENDIX A

The extrapolations of Fig. 4 were chosen to try to account for some features of the delayed $4d \rightarrow nf$ (continuum) absorption expected to be present in Cd. Measurements of the absorption coefficient $\mu$ on CdS, CdSe, and CdTe (Ref. 35) and on Sn (Ref. 36) above the $4d$ edge were not helpful as they could not be fitted well to our data. In this spectral region $n \approx 1$, so $R \approx \frac{1}{4}k^2 = h^2c^2\mu^2/64\pi^2E^2$. The delayed $d \rightarrow f$ transitions should peak 20–50 eV above threshold, producing a broad maximum in $\mu$. $R$ will peak at a much lower energy because of the factor $E^{-2}$. For extrapolation 4, $R$ peaks at 32.5 eV, giving a peak in $\mu$ around 57 eV. The sum rule on $\epsilon_2$ (using $n=1$ to get $\epsilon_2$) applied to extrapolation 4 gives about 7 electrons/atom between 30 and 60 eV, exhausting all 10 of the $4d$ electrons in the first 50 eV above threshold. This extrapolation probably is an upper limit, and may be somewhat too high. The peak at 75 eV in this extrapolation represents the excitation of the $4p$ electrons, which begins near 67 eV.[37] The lowest extrapolation, labeled 3 in Fig. 4, has no peak in $\mu$, but still includes about 5 electrons/atom in the 30–60 eV contribution to the sum rule. This extrapolation is probably too low.

## APPENDIX B

The appearance in Fig. 8 of peaks in $\epsilon_2$ that resemble those of CdO calls for further explanation, since Fig. 8 is the result of the *removal* of the effect of the oxide layer if its thickness is known. In fact, the peaks in Fig. 8 are not at the positions of peaks in $\epsilon_2$ for CdO, but are somewhat displaced. A calculation on a simple model illustrates this. If we represent the metal by a dispersionless $\tilde{\epsilon} = 0.89 + i0.87$ and the oxide by a dielectric function with a Lorentzian peak at 16.0 eV, the calculated reflectivity for a 10-Å-thick oxide layer on the metal has a peak at 15.5 eV and a minimum at 16.5 eV. KK analysis of this reflectivity, neglecting the oxide, produces an apparent $\epsilon_2$ with a peak at 14.5 eV, an energy below that of the peak in $\epsilon_2$ for the oxide. (This corresponds to a "0-Å" correction.) Correcting for 10 Å of oxide returns the flat initial (true) spectrum, while correcting for 30 Å of oxide (with 10 Å present) gives an apparent $\epsilon_2$ with a peak at 16.5 eV, higher in energy than that of the oxide $\epsilon_2$ peak. The shifts between the 0 and 30 Å peaks in Fig. 8 are less dramatic, due to overlapping structures in the oxide $\tilde{\epsilon}$, structure in the Cd $\tilde{\epsilon}$, and the appreciable similarity of the dielectric functions of Cd and CdO.

[1]R. J. Bartlett, D. W. Lynch, and R. Rosei, Phys. Rev. B 3, 4074 (1971).

[2]H. Schwarz, Phys. Stat. Solidi B 43, 755 (1971).

[3]W. C. Walker, O. P. Rustgi, and G. L. Weissler,

J. Opt. Soc. Am. 49, 471 (1959).
[4]S. Robin-Kandare, J. Robin, S. Kandare, and S. Jerič, C. R. Acad. Sci. (Paris), 257, 2026 (1963).
[5]S. Robin-Kandare, J. Robin, and S. Kandare, J. Phys. Radium 25, 218 (1964).
[6]T. M. Jelinek, R. N. Hamm, E. T. Arakawa, and R. H. Huebner, J. Opt. Soc. Am. 56, 185 (1966).
[7]S. Robin-Kandare, J. Robin, and S. Kandare, C. R. Acad. Sci. (Paris) 257, 1605 (1963).
[8]K. Codling and R. P. Madden, J. Appl. Phys. 36, 380 (1965).
[9]R. Haensel and C. Kunz, Z. Angew. Phys. 23, 276 (1967).
[10]R. P. Godwin, Springer Tracts Mod. Phys. 50, 1 (1969).
[11]C. H. Pruett (unpublished).
[12]S. S. R. Instruments, 1001 Colorado Ave., Santa Monica, Calif. 90401.
[13]Princeton Applied Research Corp., Princeton, N. J. 08540.
[14]H. Wolter in *Handbuch der Physik*, edited by S. Flügge (Springer, Berlin, 1956), Vol. XXIV, p. 461.
[15]M. Altwein, H. Finkenrath, Č. Koňák, J. Stuke, and G. Zimmerer, Phys. Status Solidi 29, 203 (1968).
[16]J. W. Osmun (unpublished).
[17]R. A. Pollak, S. Kowalczyk, L. Ley, and D. A. Shirley, Phys. Rev. Lett. 29, 274 (1972).
[18]F. Herman and S. Skillman, *Atomic Structure Calculations* (Prentice-Hall, Englewood Cliffs, N. J., 1963).
[19]T. A. Carlson, C. C. Lu, T. C. Tucker, C. W. Nestor, and F. B. Malik, Oak Ridge National Laboratory Report No. ORNL-4614, 1970 (unpublished) (quoted in Ref. 17).
[20]R. T. Poole, P. C. Kemeny, J. Liesegang, J. G. Jenkin, and R. C. G. Leckey, J. Phys. F 3, 146 (1973).
[21]R. T. Poole, R. C. G. Leckey, J. G. Jenkin, and J. Liesegang, Phys. Rev. B 8, 1401 (1973).
[22]N. J. Shevchik, J. Tejeda, M. Cardona, and D. W. Langer (unpublished).
[23]G. V. Marr and J. M. Austin, Proc. Roy. Soc. A 310, 137 (1969).
[24]D. Brust and E. O. Kane, Phys. Rev. 176, 894 (1968).
[25]J. Klima, J. Phys. C 3, 70 (1970).
[26]R. W. Stark and L. M. Falicov, Phys. Rev. Lett. 19, 795 (1967).
[27]B. Lidén, Ark. Fysik 25, 123 (1963).
[28]S. Bergwall, A. S. Nigavekar, and P. Ohlin, Ark. Fysik 40, 275 (1969).
[29]V. Hoffstein and D. S. Boudreaux, Phys. Rev. B 2, 3013 (1970).
[30]J. W. D. Connolly, Int. J. Quantum Chem. Symp. 111S, 807 (1970).
[31]U. Fano and J. W. Cooper, Rev. Mod. Phys. 40, 441 (1968).
[32]B. Feuerbacher and B. Fitton, Phys. Rev. Lett. 24, 499 (1970).
[33]C. J. Powell, Proc. Phys. Soc., Lond. 76, 593 (1960).
[34]J. L. Robins, Proc. Phys. Soc. Lond. 78, 1177 (1961).
[35]M. Cardona and R. Haensel, Phys. Rev. B 1, 2605 (1969).
[36]R. Haensel, C. Kunz, T. Sasaki, and B. Sonntag, Appl. Opt. 7, 301 (1968).
[37]J. A. Bearden and A. F. Burr, Rev. Mod. Phys. 39, 125 (1967).